Edelweiss Applied Science and Technology
ISSN: 2576-8484
Vol. 9, No. 4, 1075-1087
2025
Publisher: Learning Gate
DOI: 10.55214/25768484.v9i4.6174
© 2025 by the author; licensee Learning Gate

Effects of diamond burnishing process parameters on the surface roughness of AISI 304 austenitic stainless steel

Mariana Ichkova[1*]
[1]Department of Material Science and Mechanics of Materials Technical University of Gabrovo, 5300 Gabrovo, Bulgaria; ichkova@tugab.bg (M.I.).

Abstract: Diamond burnishing (DB) is a low-cost and reliable finishing process that dramatically improves the performance of metal components due to the favorable combination of surface integrity characteristics: a mirror-like surface, high surface microhardness, residual compressive stresses, and a grain-refined structure of the surface and nearby subsurface layers. This article aims to establish the effects of DB on surface height (Ra) and shape (Rsk and Rku) roughness parameters of 304 austenitic stainless steel specimens. DB was implemented on a CNC lathe using a spherical-ended polycrystalline diamond insert with a radius of 2 mm and flood lubrication. The steel, with a hardness of 250 HB, was tested in its as-received state. A planned experiment with a second-order composition plan, analysis of variance, and regression analyses were used to achieve the goal. The significance of the process governing factors was established via an analysis of the dimensionless absolute values of the first-order coefficients in the regression models. Explicit correlations between the main governing factors (burnishing force, feed rate, and burnishing velocity) of the DB process and the selected roughness parameters were found. The results obtained allow for the optimal selection of the DB governing factor magnitudes depending on the functional purpose of the processed component.
Keywords: *Austenitic stainless steel, Diamond burnishing, Kurtosis Roughness, Skewness, Surface integrity.*

1. Introduction

Chromium-nickel austenitic steels are widely used in many industries due to their superior general corrosion resistance, good machinability by cutting and plastic deformation, and good weldability. Besides the tendency to intergranular corrosion in the temperature range 500-700°C, another disadvantage of these steels is their insufficient hardness and strength. Overcoming this drawback is achieved by volumetric cold working [1, 2] or by modifying the surface layers (SL): low-temperature nitriding and/or carburizing to form an S-phase [3, 4] surface cold working [5, 6] or a combination of both [7, 8].

The SL of the parts are the most loaded layers, as they are exposed to external influences of different nature: the operation of the parts is associated with the transmission of power flow between their SL; the working stresses are maximum in these layers; SL are subjected to the direct impact of the environment, which is most often aggressive (for example, sea water or other chemically active environment). Therefore, the operational behavior of the parts is directly correlated with the complex state of the SL, known as surface integrity (SI), immediately after the respective finishing [9]. For example, the surface texture, and more precisely the height and shape roughness parameters skewness Rsk and kurtosis Rku, influence the tribological [10-12] and fatigue [9, 13, 14] behaviors of the corresponding metal component.

An effective approach to improve the surface texture is static surface cold working (SCW) [15]. In the static SCW, a rigid and smooth deforming element is pressed with a constant static force against the

© 2025 by the author; licensee Learning Gate
History: Received: 6 February 2025; Revised: 2 April 2025; Accepted: 7 April 2025; Published: 12 April 2025
* Correspondence: ichkova@tugab.bg

surface being machined and performs relative movement with respect to it. Thus, the surface layer is plastically deformed at a temperature lower than the recrystallization temperature of the material being processed. As a result, the roughness decreases dramatically, the surface microhardness increases significantly, beneficial residual compressive stresses are introduced into the surface and nearby subsurface layers, and the microstructure in these layers is modified in the direction of grain refinement and orientation [16]. When the tangential contact between the deforming element and the surface being machined is sliding friction, the static SCW is known as slide burnishing (SB) [17, 18]. SB is implemented with a non-diamond [19, 20] or diamond [21] deforming element. In the second case, SB is called slide diamond burnishing or diamond burnishing (DB) [17]. DB was introduced in 1962 by General Electric to improve the SI of metal components. DB is a simple and effective finishing process and its main advantage over roller burnishing [22] is the significantly simpler equipment used to perform DB. The experimental comparison between DB and deep rolling process performed in Maximov, et al. [23] showed the advantage of DB in terms of SI and fatigue strength characteristics.

Over the past six decades, DB has established itself as an effective finish for structural [24] tool [25] and stainless [10, 26] steels, high-strength titanium [27] and aluminum [28, 29] alloys, bronze [30] and other alloys.

Extensive studies on the influence of governing factors of the DB process on the roughness parameters of samples made of chromium-nickel austenitic steels have been conducted in Korzynski, et al. [10]; Maximov, et al. [16]; Maximov, et al. [26]; Korzynski, et al. [31] and Skoczylas, et al. [32]. The emphasis in these studies was placed primarily on the DB–Ra roughness parameter correlation. Explicit correlations between SI characteristics and fatigue limit of diamond burnished AISI 304 chromium-nickel austenitic stainless steels were established in Maximov, et al. [9]. However, there is no information regarding the influence of the governing factors of the DB process on the shape roughness parameters skewness and kurtosis, which have a significant impact on the operational behavior (fatigue and wear) of the respective component. The availability of such information will allow for the correct selection of the values of the governing factors of the DB process, so as to achieve the desired operational behavior of the diamond burnished metal component.

Thus, the aim of the study is to find explicit dependencies between the main governing factors of DB of AISI 304 stainless steel and Ra, Rsk and Rku roughness parameters.

2. Materials and Methods

AISI 304 chromium-nickel austenitic stainless steel was chosen because this grade is most commonly used in engineering practice. The material was received as hot-rolled bars with diameters of 16 mm and was used in as-received state. The chemical composition was established using optical emission spectrometer. Tensile tests at room temperature were carried out via Zwick/Roell Vibrophore 100 testing machine. The working sections of the tensile test specimens have a diameter of 6 mm and a length of 30 mm. The material hardness was measured via a VEB-WPM tester using a spherical-ended indenter having a diameter of 2.5 mm, loading of 63 kg, and holding time of 10 s.

DB was implemented on Index Traub CNC lathe using spherical-ended polycrystalline diamond insert with radius of 2 mm and conventional flood lubrication (Vasco 6000). The governing factors were burnishing force F_b, feed rate f, and burnishing velocity v (Figure 1a).

Edelweiss Applied Science and Technology
ISSN: 2576-8484
Vol. 9, No. 4: 1075-1087, 2025
DOI: 10.55214/25768484.v9i4.6174
© 2025 by the author; licensee Learning Gate

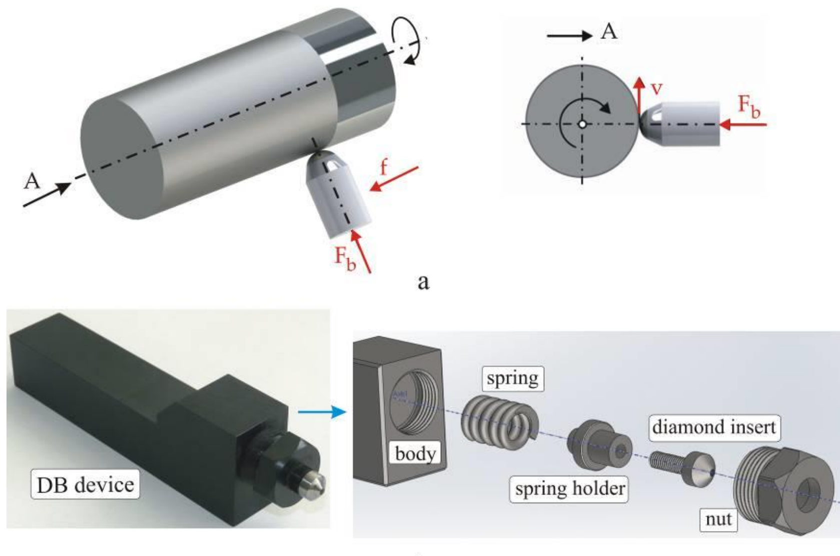

Figure 1.
DB implementation: a. kinematics and governing factors; b. DB device.

The governing factor magnitudes (Table 1) were selected based on the results obtained in [26] via one-factor-at-a-time method. The transformation from physical (natural) $\tilde{x}_i$ to coded (dimensionless) x_i variables is done by the formula:

$$x_i = \frac{\left(\tilde{x}_i - \tilde{x}_{i,0}\right)}{\left(\tilde{x}_{i,max} - \tilde{x}_{i,0}\right)}, \qquad (1)$$

where $\tilde{x}_{i,0}$ and $\tilde{x}_{i,max}$ are respectively the average and maximum value of the physical variable. The inverse transformation $x_i \to \tilde{x}_i$ is obtained from the formula:

$$\tilde{x}_i = \left(\tilde{x}_{i,max} - \tilde{x}_{i,0}\right)x_i + \tilde{x}_{i,0}. \qquad (2)$$

The objective functions were Ra, Rsk and Rku roughness parameters: Y_{Ra}, Y_{sk} and Y_{ku}, respectively. The reason for choosing these three parameters is as follows: 1) Ra roughness parameter is a representative of the height (amplitude) roughness parameters and is the most used roughness parameter in engineering practice.; 2) The shape roughness parameters (skewness and kurtosis) play a significant role in the operational behavior of the diamond burnished surface [9, 11-13]. Ra and Rku are positive, while the skewness can be positive, negative, or equal to zero.

The used burnishing device (Fig. 1b) provides elastic normal contact between the deforming element and the burnished surface. Turning as premachining and DB were carried out on CNC lathe in one clamping process to minimize the concentric run-out in DB. VCMT 160404 – F3P carbide cutting insert (main back angle $\alpha_0 = 7^o$; radius at tool tip 0.4 mm) was used for the previous turning. SVJCR 2525M-16 holder with main and auxiliary setting angles, $\chi_c = 93^o$ and $\chi'_c = 52^o$ respectively, was used. The cutting insert and the holder are manufactured by ISCAR Bulgaria. The average value of Ra roughness parameter before DR was $Ra^{init} = 0.529\ \mu m$.

© 2025 by the author; licensee Learning Gate

Table 1.
Governing factors and their levels.

Governing factors	Levels							
	Natural, $\tilde{x}_i$				Coded, x_i			
Burnishing force F_b $[N]$	$\tilde{x}_1$	100	300	500	x_1	-1	0	1
Feed rate f $[mm/rev]$	$\tilde{x}_2$	0.02	0.05	0.08	x_2	-1	0	1
Burnishing velocity v [m/min]	$\tilde{x}_3$	50	85	120	x_3	-1	0	1

2D roughness parameters were measured using a Mitutoyo Surftest SJ-210 surface roughness tester and 0.8 mm base length. The final results were obtained as average arithmetic values from the measurements on six equally spaced sample generatrixes.

3. Results and Discussion

3.1. Material used

Table 2 shows the chemical composition of the used AISI 304 stainless steel. The remaining chemical elements (0.203 wt%) are Ti, Al, Pb, Sn, Nb, B, As, Zn, Bi, Zr and Ca. The main mechanical characteristics in as-received state of the material are shown in Table 3.

Table 2.
Chemical composition (in wt%) of the used AISI 304 stainless steel.

Fe	C	Si	Mn	P	S	Cr	Ni	Mo	Cu	Co	V	W	other
69.51	0.023	0.271	1.600	0.047	0.034	19.19	7.98	0.243	0.637	0.161	0.060	0.041	Balance

Table 3.
Main mechanical characteristics of the tested AISI 304 stainless steel (as-received).

Yield limit, MPa	Tensile strength, MPa	Elongation, %	Hardness, HB
338^{+9}_{-18}	733^{+12}_{-10}	$44.7^{+0.3}_{-0.2}$	$250^{\pm 8}$

3.2. Experimental Design and Results

A planned experiment and a second-order optimal composition design were used (Table 4).

The obtained experimental results are shown in Table 4. Regression analyzes were performed using QStatLab software [33]. Given the chosen experimental design, the approximating polynomials are of the order no higher than the second:

$$Y^{(k)}(\{X\}) = b_0^{(k)} + \sum_{i=1}^{3} b_i^{(k)} x_i + \sum_{i=1}^{2} \sum_{j=i-1}^{3} b_{ij}^{(k)} x_i x_j + \sum_{i=1}^{3} b_{ii}^{(k)} x_i^2 , k = 1,2,3, \quad (3)$$

where $\{X\}$ is the vector of the governing factors x_i, and $k = 1,2,3$ shows the corresponding objective function: Y_{Ra}, Y_{sk} and Y_{ku}, respectively.

The polynomial coefficients of the three models (Ra, Rsk and Rku) are shown in Table 5. Table 4 shows the values predicted by the models at the experimental points. The comparison with experimental results shows good agreement between the models and the experiment.

Edelweiss Applied Science and Technology
ISSN: 2576-8484
Vol. 9, No. 4: 1075-1087, 2025
DOI: 10.55214/25768484.v9i4.6174
© 2025 by the author; licensee Learning Gate

Table 4.
Experimental design and results.

№	x_1	x_2	x_3	Ra, μm		Rsk		Rku	
				Experim.	Y_{Ra} **model**	**Experim.**	Y_{sk} **model**	**Experim.**	Y_{ku} **model**
1	-1	-1	-1	0.176	0.182	-0.149	-0.354	3.090	3.438
2	1	-1	-1	0.249	0.264	0.512	0.371	7.833	8.438
3	-1	1	-1	0.268	0.271	-0.073	-0.025	2.202	1.311
4	1	1	-1	0.328	0.315	0.723	0.900	2.747	2.832
5	-1	-1	1	0.187	0.199	-0.144	-0.321	2.973	2.888
6	1	-1	1	0.339	0.335	-0.024	-0.071	5.551	6.441
7	-1	1	1	0.279	0.263	0.012	0.153	2.384	1.779
8	1	1	1	0.367	0.361	0.399	0.604	2.203	1.854
9	-1	0	0	0.224	0.217	0.189	0.383	2.875	4.106
10	1	0	0	0.302	0.308	1.165	0.971	7.876	6.644
11	0	-1	0	0.171	0.141	-0.549	-0.477	12.951	11.191
12	0	1	0	0.168	0.198	0.598	0.026	6.075	7.834
13	0	0	-1	0.147	0.133	-0.204	-0.082	4.774	4.625
14	0	0	1	0.151	0.164	-0.091	-0.213	3.712	3.861
T				0.529		0.490		2.613	

Note: T - after fine turning (i.e., before DB)

Table 5.
Regression coefficients.

Y_κ	$b_0^{(k)}$	$b_1^{(k)}$	$b_2^{(k)}$	$b_3^{(k)}$	$b_{11}^{(k)}$	$b_{22}^{(k)}$	$b_{33}^{(k)}$	$b_{12}^{(k)}$	$b_{23}^{(k)}$	$b_{13}^{(k)}$
Y_{Ra}	0.15369	0.04510	0.0288	0.0155	0.10931	0.01581	-0.0047	-0.0096	-0.00637	0.013375
Y_{Rsk}	0.07350	0.2940	0.2513	-0.066	0.6035	-0.2990	-0.2210	0.05025	0.0365	-0.11875
Y_{Rku}	7.75431	1.2686	-1.679	-0.382	-2.3788	1.75869	-3.5113	-0.8696	0.254625	-0.36138

3.3. Discussion

The dimensionless absolute values of the coefficients b_i indicate the significance of the corresponding governing factor. The greater this value, the stronger the influence of the respective governing factor. The burnishing force has the strongest influence on the Ra roughness parameter ($b_1^{(1)} = 0.0451$) and the influence of the burnishing velocity is the weakest ($b_3^{(1)} = 0.0155$). The feed rate occupies an intermediate position, somewhat closer to burnishing velocity. The skewness is most strongly influenced by burnishing force $\left(b_1^{(2)} = 0.2940\right)$ while the influence of burnishing velocity is negligible $\left(\left|b_3^{(2)}\right| = 0.066\right)$. The feed rate also has a strong influence on the skewness, although slightly less than that of the burnishing force. The feed rate has a strong influence on the kurtosis $\left(\left|b_2^{(3)}\right| = 1.679\right)$, followed by the burnishing force $\left(b_1^{(3)} = 1.2686\right)$. The absolute value of the coefficient $b_3^{(3)}$ is the smallest $\left(\left|b_3^{(3)}\right| = 0.382\right)$, but the coefficient $b_{33}^{(3)}$ has the largest absolute value compared to all other coefficients (except $b_0^{(3)}$) in the kurtosis model. So, using the method of comparing dimensionless coefficients, it is difficult to assess the significance of the factors in the kurtosis

ISSN: 2576-8484
Vol. 9, No. 4: 1075-1087, 2025
DOI: 10.55214/25768484.v9i4.6174
© 2025 by the author; licensee Learning Gate

model. Therefore, an analysis of variance (ANOVA) using QStatLab was performed. The results are shown in Figures 2, 3 and 4.

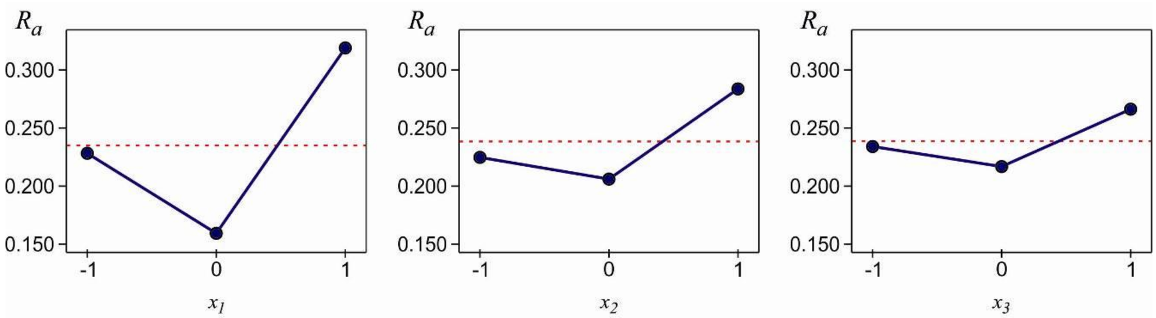

Figure 2.
ANOVA outcomes: main effects for the Ra model.

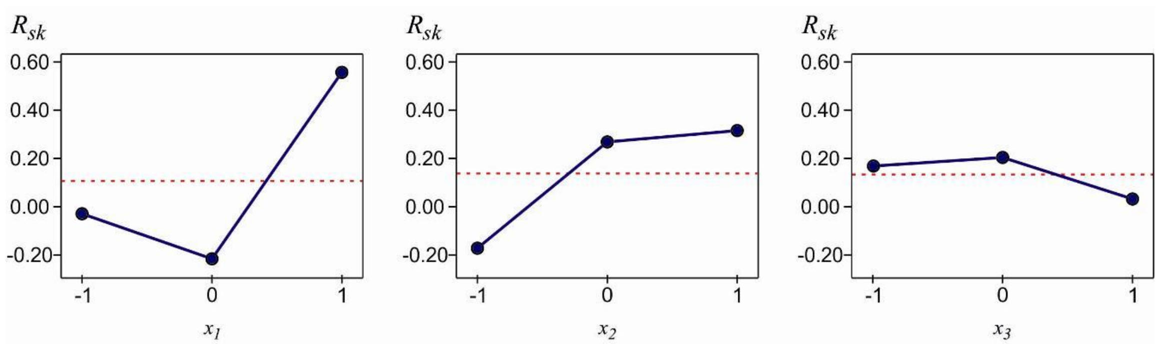

Figure 3.
ANOVA outcomes: main effects for the skewness Rsk model.

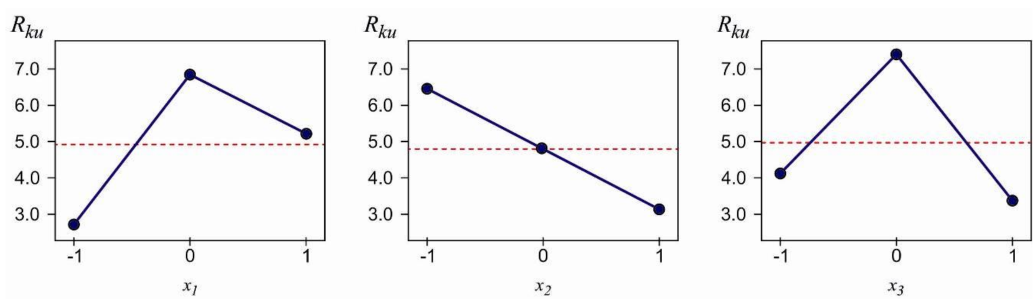

Figure 4.
ANOVA outcomes: main effects for the kurtosis Rku model.

The ANOVA outcomes confirm the conclusions drawn about the significance of the governing factors in the models of Ra (Figure 2) and Rsk (Figure 3) roughness parameters, and show that in the kurtosis model (Figure 4) the most significant governing factor is burnishing velocity, and the least significant factor is feed rate.

Graphical visualizations of the three models are shown in Figures 5, 6 and 7. The visual inspection confirms the conclusions drawn about the significance of the governing factors.

© 2025 by the author; licensee Learning Gate

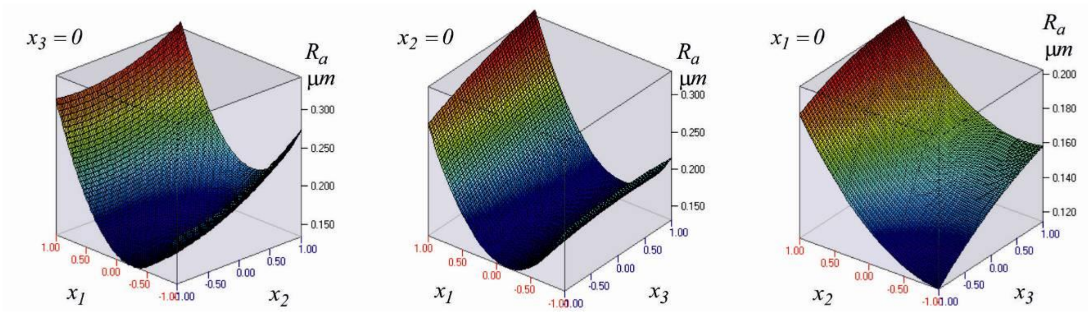

Figure 5.
Graphical visualization of the model of Ra roughness parameter.

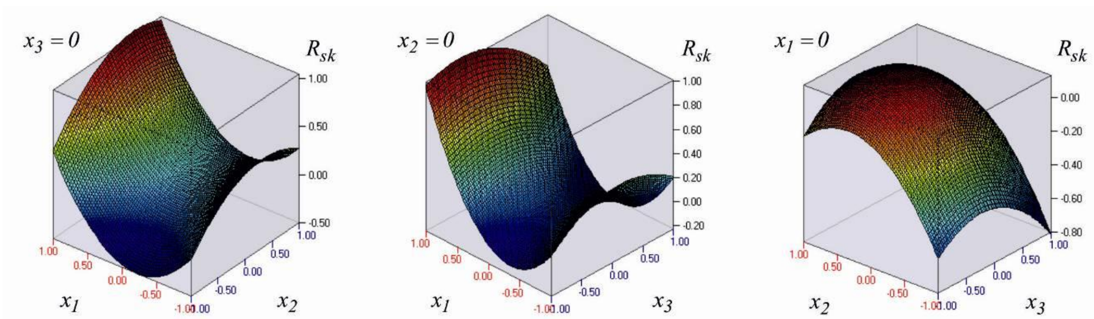

Figure 6.
Graphical visualization of the model of Rsk roughness parameter.

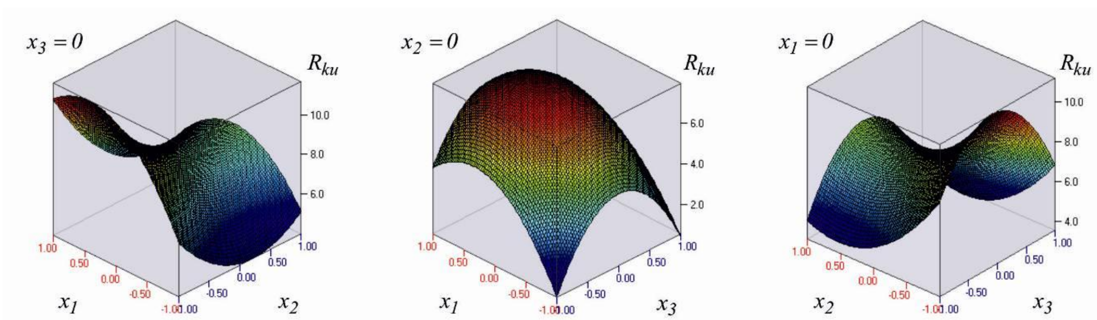

Figure 7.
Graphical visualization of the model of Rku roughness parameter.

After substituting (1) into (3), the dependencies of the objective functions on the physical variables are obtained. Figures 8, 9 and 10 show cross-sections of the objective function surfaces via characteristic planes. These cross-sections visualize the dependence of each of the objective functions on the corresponding governing factor.

The dependence of the Ra roughness parameter on burnishing force for different combinations of the other two governing factors shows a clearly pronounced minimum when $F_b = 250\ N$ (Figure 8). Lower values of the burnishing force are obviously insufficient for plastic deformation of the peaks. However, values above 300 N deteriorate the height roughness parameters. For all combinations of burnishing force and burnishing velocity, the roughness parameter Ra increases with increasing feed rate, with the minimum roughness Ra occurring when the feed rate takes a minimum value. It should be noted that with increasing the feed rate the velocity of increase of the Ra parameter increases, which confirms the observation made by Nestler and Schubert [34]. The influence of burnishing velocity on Ra is similar to that of feed rate, but is less pronounced. For the entire range of feed rate variation, Ra

© 2025 by the author; licensee Learning Gate

increases slightly with increasing burnishing force. However, the increase in Ra is not uniform for different values of burnishing force: With increasing burnishing force, the influence of burnishing velocity on Ra increases.

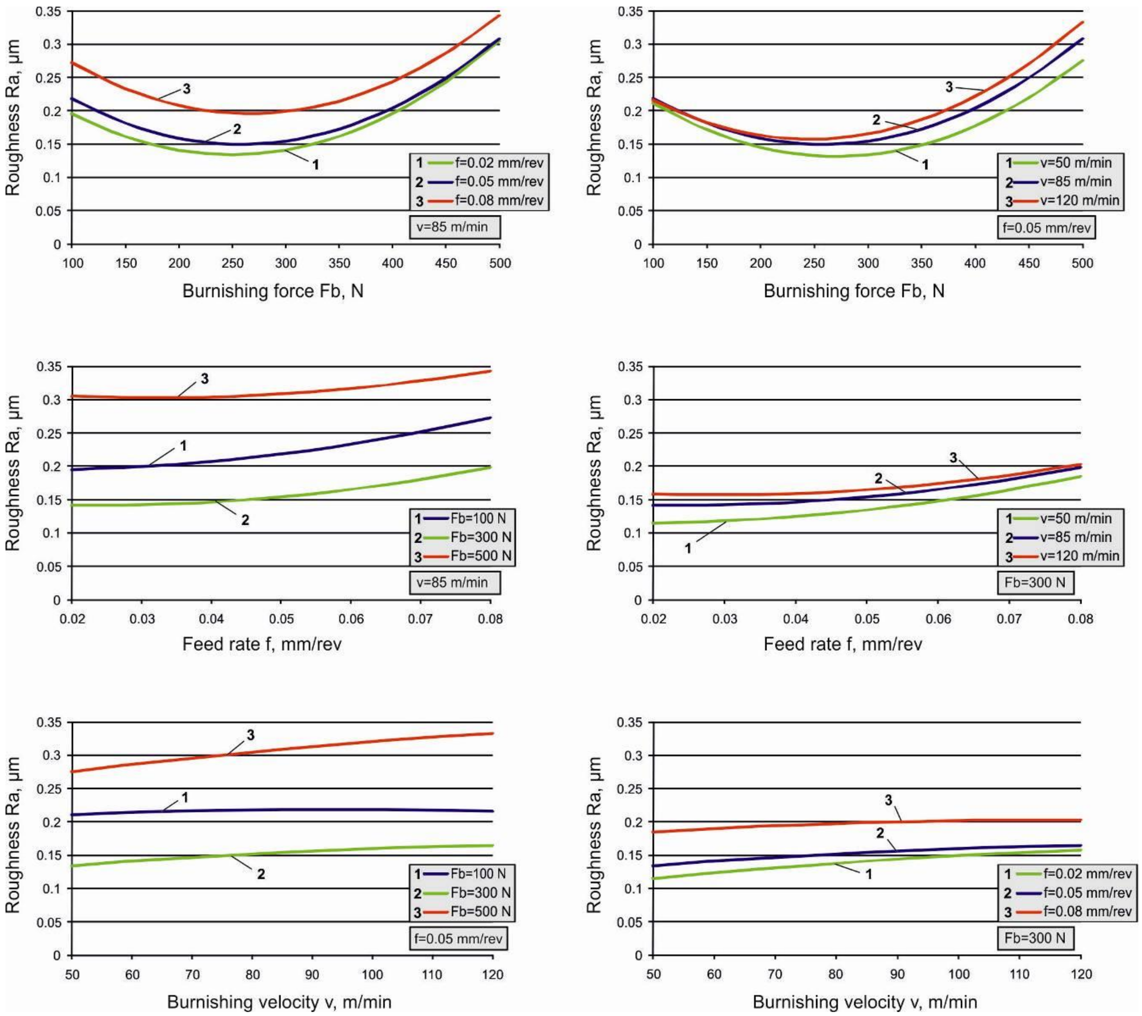

Figure 8.
Dependence of Ra roughness parameter on DB process governing factors.

The skewness shows a clear minimum when the burnishing force is in the range of 230 – 280 N, for all combinations of feed rate and burnishing velocity (Figure 9). The combination of minimum feed rate and $F_b < 450\ N$ provides negative skewness, which is essential when the diamond burnished surface should ensure increased wear resistance under boundary lubrication friction conditions [11, 12, 35]. As the feed rate increases to approximately $f = 0.065\ mm/rev$, the skewness increases (as an algebraic number), then decreases slightly. The influence of burnishing velocity on the skewness is similar, but less pronounced. The skewness is minimal when the burnishing velocity is maximal. When the feed rate is minimal and the burnishing force is around the middle of the interval (i.e., $F_b = 300\ N$), the skewness is negative for the entire range of burnishing velocity variation.

© 2025 by the author; licensee Learning Gate

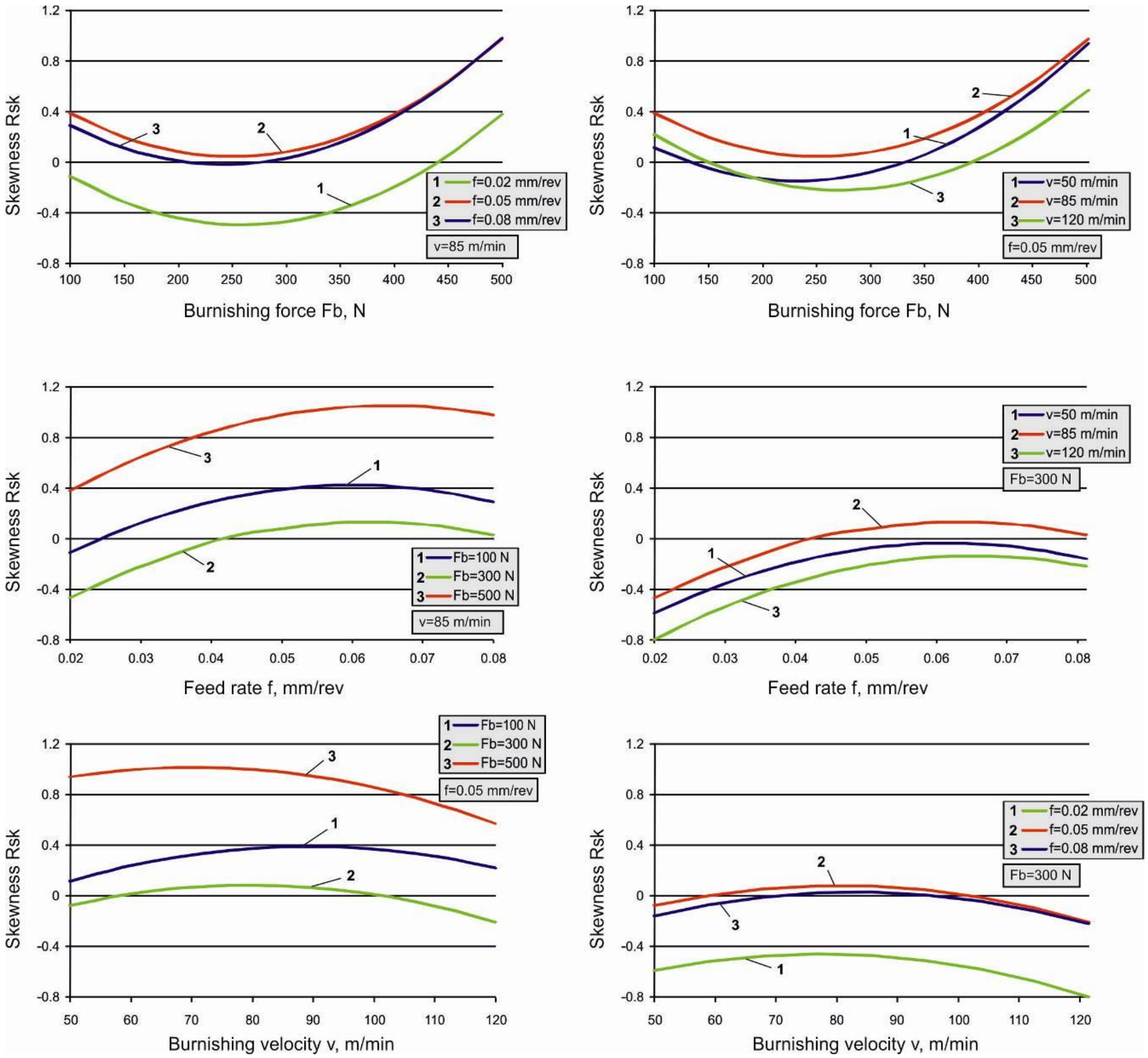

Figure 9.
Dependence of the skewness Rsk roughness parameter on DB process governing factors.

With increasing burnishing force to approximately 340 N – 370 N, the kurtosis increases, then gradually decreases (Figure 10). Conversely, as the feed rate increases to approximately 0.065 mm/rev, the kurtosis decreases, then gradually increases. Minimum feed rate provides maximum kurtosis. As the burnishing velocity increases to the middle of the interval (i.e., $v = 85\ m/min$), the kurtosis increases, then decreases.

It should be noted that the conclusions drawn are only valid for the radius of the diamond insert $r = 2\ mm$ (such as was used in the experiment) and for the intervals of variation of the variables shown in Table 2.

ISSN: 2576-8484
Vol. 9, No. 4: 1075-1087, 2025
DOI: 10.55214/25768484.v9i4.6174
© 2025 by the author; licensee Learning Gate

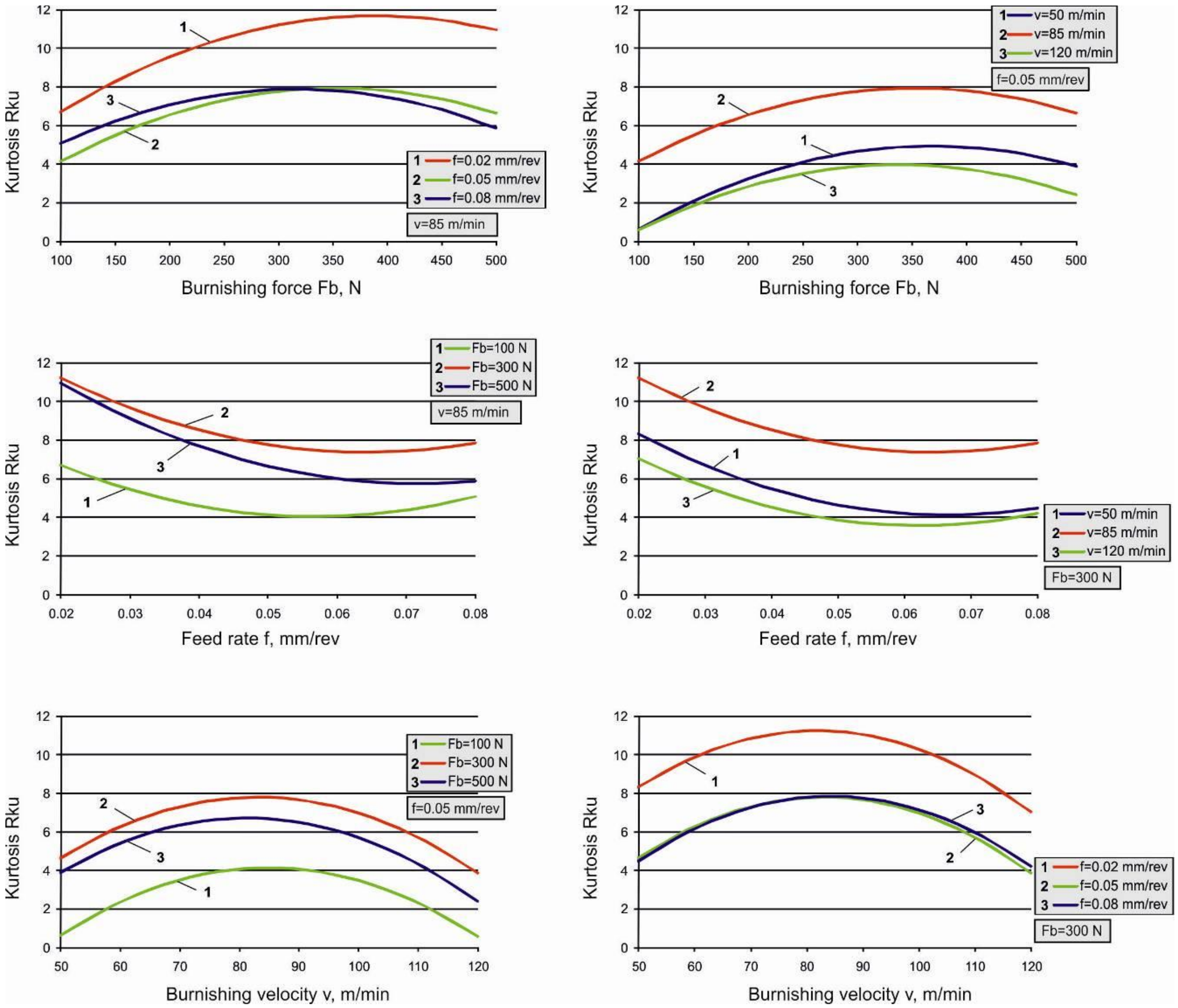

Figure 10.
Dependence of the kurtosis Rku roughness parameter on DB process governing factors.

4. Conclusions

As a result of this work, the major new findings concerning the nature of DB process were:

- Explicit correlations between the main process parameters DB of AISI 304 steel specimens and Ra, Rsk and Rku roughness parameters were established.
- The dependence of Ra on burnishing force shows a clear minimum around $F_b = 250\ N$ (Figure 8). The roughness parameter Ra increases with increasing feed rate, with the minimum roughness Ra occurring when the feed rate is at its minimum value. The effect of burnishing velocity on Ra is similar to that of feed rate, but is less pronounced.
- The skewness has a minimum when the burnishing force is in the interval 230 N – 280 N. The combination of minimal feed rate and $F_b < 450\ N$ provides negative skewness. By increasing the feed rate to about $f = 0.065\ mm/rev$ the skewness increases, then slightly decreases. Similarly, but less pronounced is the influence of burnishing velocity on the skewness.
- The kurtosis reaches its maximum value when the burnishing force is in the range of 340 N – 370 N, after which it gradually decreases. Minimum feed rate provides maximum kurtosis. As the feed

Edelweiss Applied Science and Technology
ISSN: 2576-8484
Vol. 9, No. 4: 1075-1087, 2025
DOI: 10.55214/25768484.v9i4.6174
© 2025 by the author; licensee Learning Gate

rate increases to about 0.065 mm/rev, the kurtosis decreases, then gradually increases. Burnishing velocity has a significant effect on the kurtosis. As the velocity increases to the middle of the interval ($v = 85\ m/min$), the kurtosis increases, then decreases.

- The results obtained allow for optimal selection of the DB governing factor magnitudes depending on the functional purpose of the processed component.

Abbreviations:

ANOVA	Analysis of variance
CNC	Computer numerical control
DB	Diamond burnishing
NSGA	Non-dominated sorting genetic algorithm
SB	Slide burnishing
SCW	Surface cold working
SI	Surface integrity
SL	Surface layers

List of symbols:

f	Feed rate
F_b	Burnishing force
Ra	Arithmetic average of roughness profile
Rsk	Skewness
Rku	Kurtosis
v	Burnishing velocity
x_i	Variable in coded form
$\tilde{x}_i$	Variable in natural form
$\{X\}$	Vector of the governing factors
$\{X\}^*$	Vector of the optimal values of the governing factors
Y_i	Objective function
α_0	Main back angle
χ_c	Main setting angle
χ_c'	Auxiliary setting angle

Funding:

This research was funded by the European Regional Development Fund under the Operational Program"Scientific Research, Innovation and Digitization for Smart Transformation 2021–2027", Project CoC "Smart Mechatronics, Eco- and Energy Saving Systems and Technologies", BG16RFPR002-1.014-0005.

Transparency:

The author confirms that the manuscript is an honest, accurate, and transparent account of the study; that no vital features of the study have been omitted; and that any discrepancies from the study as planned have been explained. This study followed all ethical practices during writing.

© 2025 by the author; licensee Learning Gate

Copyright:
© 2025 by the authors. This open-access article is distributed under the terms and conditions of the Creative Commons Attribution (CC BY) license (https://creativecommons.org/licenses/by/4.0/).

References

[1] A. Hedayati, A. Najafizadeh, A. Kermanpur, and F. Forouzan, "The effect of cold rolling regime on microstructure and mechanical properties of AISI 304L stainless steel," *Journal of Materials Processing Technology*, vol. 210, no. 8, pp. 1017-1022, 2010. https://doi.org/10.1016/j.jmatprotec.2010.02.010
[2] B. R. Kumar, A. Singh, S. Das, and D. Bhattacharya, "Cold rolling texture in AISI 304 stainless steel," *Materials Science and Engineering: A*, vol. 364, no. 1-2, pp. 132-139, 2004. https://doi.org/10.1016/j.msea.2003.08.012
[3] F. Borgioli, "From austenitic stainless steel to expanded austenite-S phase: formation, characteristics and properties of an elusive metastable phase," *Metals*, vol. 10, no. 2, p. 187, 2020. https://doi.org/10.3390/met10020187
[4] Y. Hoshiyama, R. Mizobata, and H. Miyake, "Mechanical properties of austenitic stainless steel treated by active screen plasma nitriding," *Surface and Coatings Technology*, vol. 307, pp. 1041-1044, 2016. https://doi.org/10.1016/j.surfcoat.2016.07.032
[5] P. Juijerm and I. Altenberger, "Fatigue performance enhancement of steels using mechanical surface treatments," *Journal of Metals, Materials and Minerals*, vol. 17, no. 1, pp. 59–65, 2007.
[6] I. Nikitin and I. Altenberger, "Comparison of the fatigue behavior and residual stress stability of laser-shock peened and deep rolled austenitic stainless steel AISI 304 in the temperature range 25–600 C," *Materials Science and Engineering: A*, vol. 465, no. 1-2, pp. 176-182, 2007. https://doi.org/10.1016/j.msea.2007.02.004
[7] Y. Lin, J. Lu, L. Wang, T. Xu, and Q. Xue, "Surface nanocrystallization by surface mechanical attrition treatment and its effect on structure and properties of plasma nitrided AISI 321 stainless steel," *Acta Materialia*, vol. 54, no. 20, pp. 5599-5605, 2006. https://doi.org/10.1016/j.actamat.2006.08.014
[8] J. Maximov, G. Duncheva, A. Anchev, V. Dunchev, and Y. Argirov, "Improvement in fatigue strength of chromium–nickel austenitic stainless steels via diamond burnishing and subsequent low-temperature gas nitriding," *Applied Sciences*, vol. 14, no. 3, p. 1020, 2024. http://doi.org/10.3390/app14031020
[9] J. T. Maximov, G. V. Duncheva, A. P. Anchev, and V. P. Dunchev, "Explicit correlation between surface integrity and fatigue limit of surface cold worked chromium-nickel austenitic stainless steels," *The International Journal of Advanced Manufacturing Technology*, vol. 133, no. 11, pp. 6041-6058, 2024. http://dx.doi.org/10.1007/s00170-024-14113-6
[10] M. Korzynski, K. Dudek, B. Kruczek, and P. Kocurek, "Equilibrium surface texture of valve stems and burnishing method to obtain it," *Tribology International*, vol. 124, pp. 195-199, 2018. https://doi.org/10.1016/j.triboint.2018.04.014
[11] M. Sedlaček, B. Podgornik, and J. Vižintin, "Correlation between standard roughness parameters skewness and kurtosis and tribological behaviour of contact surfaces," *Tribology international*, vol. 48, pp. 102-112, 2012. https://doi.org/10.1016/j.triboint.2011.11.008
[12] G. Duncheva, J. Maximov, A. Anchev, V. Dunchev, Y. Argirov, and M. Kandeva-Ivanova, "Enhancement of the wear resistance of CuAl9Fe4 sliding bearing bushings via diamond burnishing," *Wear*, vol. 510, p. 204491, 2022. https://doi.org/10.1016/j.wear.2022.204491
[13] A. Zabala, L. Blunt, W. Tato, A. Aginagalde, X. Gomez, and I. Llavori, "The use of areal surface topography characterisation in relation to fatigue performance," in *MATEC Web of Conferences*, 2018, vol. 165: EDP Sciences, p. 14013.
[14] J. Zhang and Z. Pei, *Characterization methods for surface integrity* (Surface Integrity in Machining). London: Springer, 2010.
[15] G. Duncheva and J. Maximov, "Cold working technologies for increasing the fatigue life of metal structural components with fastener holes—review and perspectives," *The International Journal of Advanced Manufacturing Technology*, vol. 136, pp. 1-35, 2025. https://doi.org/10.1007/s00170-025-15020-0
[16] J. Maximov, G. Duncheva, A. Anchev, V. Dunchev, Y. Argirov, and M. Nikolova, "Effects of heat treatment and diamond burnishing on fatigue behaviour and corrosion resistance of AISI 304 austenitic stainless steel," *Applied Sciences*, vol. 13, no. 4, p. 2570, 2023. https://doi.org/10.3390/app13042570
[17] M. Korzynski, *Slide diamond burnishing* (Nonconventional finishing technologies). Warsaw, 2013, pp. 9-33.
[18] H. Roohi, H. Baseri, and M. J. Mirnia, "Evaluation of optimized surface characteristics in non-rotational sliding ball burnishing," *Materials and Manufacturing Processes*, vol. 39, no. 16, pp. 2299-2308, 2024. https://doi.org/10.1080/10426914.2024.2395010
[19] J. Maximov, T. Kuzmanov, G. Duncheva, and N. Ganev, "Spherical motion burnishing implemented on lathes," *International Journal of Machine Tools and Manufacture*, vol. 49, no. 11, pp. 824-831, 2009. https://doi.org/10.1016/j.ijmachtools.2009.05.011
[20] J. Maximov and G. Duncheva, "Finite element analysis and optimization of spherical motion burnishing of low-alloy steel," *Proceedings of the Institution of Mechanical Engineers, Part C: Journal of Mechanical Engineering Science*, vol. 226, no. 1, pp. 161-176, 2012. https://doi.org/10.1177/0954406211412024

[21] E. H. Hull and A. J. Nerad, *U.S. Patent No. 2,966,722*. Washington, DC: U.S. Patent and Trademark Office, 1961.

[22] G. Duncheva, J. Maximov, V. Dunchev, A. Anchev, T. Atanasov, and J. Capek, "Single toroidal roller burnishing of 2024-T3 Al alloy implemented as mixed burnishing process," *The International Journal of Advanced Manufacturing Technology*, vol. 111, pp. 3559-3570, 2020. https://doi.org/10.1007/s00170-020-06350-2

[23] J. Maximov, G. Duncheva, A. Anchev, and V. Dunchev, "Slide burnishing versus deep rolling—A comparative analysis," *The International Journal of Advanced Manufacturing Technology*, vol. 110, pp. 1923-1939, 2020.

[24] J. Maximov, G. Duncheva, A. Anchev, and V. Dunchev, "Smoothing, deep, or mixed diamond burnishing of low-alloy steel components–optimization procedures," *The International Journal of Advanced Manufacturing Technology*, vol. 106, pp. 1917-1929, 2020.

[25] D. Toboła and B. Kania, "Phase composition and stress state in the surface layers of burnished and gas nitrided Sverker 21 and Vanadis 6 tool steels," *Surface and Coatings Technology*, vol. 353, pp. 105-115, 2018. https://doi.org/10.1016/j.surfcoat.2018.08.055

[26] J. Maximov, G. Duncheva, A. Anchev, V. Dunchev, and Y. Argirov, "Effect of diamond burnishing on fatigue behaviour of AISI 304 chromium-nickel austenitic stainless steel," *Materials*, vol. 15, no. 14, p. 4768, 2022. https://doi.org/10.3390/ma15144768

[27] D. Toboła, J. Morgiel, and Ł. Maj, "TEM analysis of surface layer of Ti-6Al-4V ELI alloy after slide burnishing and low-temperature gas nitriding," *Applied Surface Science*, vol. 515, p. 145942, 2020. https://doi.org/10.1016/j.apsusc.2020.145942

[28] J. Maximov, A. Anchev, V. Dunchev, N. Ganev, G. Duncheva, and K. Selimov, "Effect of slide burnishing basic parameters on fatigue performance of 2024-T3 high-strength aluminium alloy," *Fatigue & Fracture of Engineering Materials & Structures*, vol. 40, no. 11, pp. 1893-1904, 2017. https://doi.org/10.1111/ffe.12608

[29] J. T. Maximov, A. P. Anchev, G. V. Duncheva, N. Ganev, K. F. Selimov, and V. P. Dunchev, "Impact of slide diamond burnishing additional parameters on fatigue behaviour of 2024-T3 Al alloy," *Fatigue & Fracture of Engineering Materials & Structures*, vol. 42, no. 1, pp. 363-373, 2019. https://doi.org/10.1111/ffe.12915

[30] G. V. Duncheva, J. T. Maximov, A. P. Anchev, V. P. Dunchev, and Y. B. Argirov, "Multi-objective optimization of the internal diamond burnishing process," *Materials and Manufacturing Processes*, vol. 37, no. 4, pp. 428-436, 2022. https://doi.org/10.1080/10426914.2021.1981937

[31] M. Korzynski, K. Dudek, and K. Korzynska, "Effect of slide diamond burnishing on the surface layer of valve stems and the durability of the stem-graphite seal friction pair," *Applied Sciences*, vol. 13, no. 11, p. 6392, 2023. https://doi.org/10.3390/app13116392

[32] A. Skoczylas, K. Zaleski, J. Matuszak, K. Ciecieląg, R. Zaleski, and M. Gorgol, "Influence of slide burnishing parameters on the surface layer properties of stainless steel and mean positron lifetime," *Materials*, vol. 15, no. 22, p. 8131, 2022. https://doi.org/10.3390/ma15228131

[33] I. N. Vuchkov and I. I. Vuchkov, *QStatLab professional, v. 5.5–statistical quality control software*. Bulgaria: User's Manual. Sofia, 2009.

[34] A. Nestler and A. Schubert, "Effect of machining parameters on surface properties in slide diamond burnishing of aluminium matrix composites," *Materials Today: Proceedings*, vol. 2, pp. S156-S161, 2015. https://doi.org/10.1016/j.matpr.2015.05.033

[35] G. Duncheva, J. Maximov, A. Anchev, V. Dunchev, and Y. B. Argirov, "Improvement in wear resistance performance of CuAl8Fe3 single-phase aluminum bronze via slide diamond burnishing," *Journal of Materials Engineering and Performance*, vol. 31, no. 3, pp. 2466-2478, 2022. http://dx.doi.org/10.1007/s11665-021-06389-6

Edelweiss Applied Science and Technology
ISSN: 2576-8484
Vol. 9, No. 4: 1075-1087, 2025
DOI: 10.55214/25768484.v9i4.6174

© 2025 by the author; licensee Learning Gate